International Journal of Psychophysiology 97 (2015) 299–309

Contents lists available at ScienceDirect

International Journal of Psychophysiology

journal homepage: www.elsevier.com/locate/ijpsycho

Posterior EEG alpha at rest and during task performance: Comparison of current source density and field potential measures

Craig E. Tenke [a,b,*], Jürgen Kayser [a,b], Karen Abraham [a], Jorge E. Alvarenga [a], Gerard E. Bruder [a,b]

[a] Division of Cognitive Neuroscience, New York State Psychiatric Institute, New York, NY, USA
[b] Department of Psychiatry, Columbia University College of Physicians & Surgeons, New York, NY, USA

ARTICLE INFO

Article history:
Received 8 January 2015
Received in revised form 19 May 2015
Accepted 22 May 2015
Available online 27 May 2015

Keywords:
Surface Laplacian
Current source density (CSD)
Recording reference
EEG alpha
Event related desynchronization (ERD)
Individual differences

ABSTRACT

Resting and task-related EEG alpha are used in studies of cognition and psychopathology. Although Laplacian methods have been applied, apprehensions about loss of global activity dissuade researchers from greater use except as a supplement to reference-dependent measures. The unfortunate result has been continued reliance on reference strategies that differ across labs, and a systemic preference for a montage-dependent average reference over true reference-free measures. We addressed these concerns by comparing resting- and task-related EEG alpha using three EEG transformations: nose- (NR) and average-referenced (AR) EEG, and the corresponding CSD. Amplitude spectra of resting and prestimulus task-related EEG (novelty oddball) and event-related spectral perturbations were scaled to equate each transformation. Alpha measures quantified for 8–12 Hz bands were: 1) net amplitude (eyes-closed minus eyes-open) and 2) overall amplitude (eyes-closed plus eyes-open); 3) task amplitude (prestimulus baseline) and 4) task event-related desynchronization (ERD). Mean topographies unambiguously represented posterior alpha for overall, net and task, as well as poststimulus alpha ERD. Topographies were similar for the three transformations, but differed in dispersion, CSD being sharpest and NR most broadly distributed. Transformations also differed in scale, AR showing less attenuation or spurious secondary maxima at anterior sites, consistent with simulations of distributed posterior generators. Posterior task alpha and alpha ERD were positively correlated with overall alpha, but not with net alpha. CSD topographies consistently and appropriately represented posterior EEG alpha for all measures.

Published by Elsevier B.V.

1. Introduction

The alpha rhythm of the EEG has classically been identified as a cortical idling rhythm, and putative homologs in nonhuman mammals have greatly informed our understanding of thalamocortical organization (Gloor, 1969; Steriade, 2000; Steriade et al., 1993). Alpha blockade with attention has been widely used as a neurophysiological measure of activation, ranging in scale and scope from task-related local cortical desynchronization to the more general relaxation or arousal of an individual at rest (Babiloni et al., 2014; Kayser et al., 2014; Klimesch, 2012). Not surprisingly, a number of reports have identified a correspondence between prestimulus alpha and poststimulus processing, as evidenced by subsequent task-related ERP components (e.g., Jasiukaitis and Hakerem, 1988; Barry et al, 2000). However, the implications of a resting alpha blockade and alpha ERD are considerably different: while the former is a measure of arousal from relaxation, the latter may be viewed as an index of top-down processes associated with attention (von Stein et al., 2000; Kayser et al., 2014). A related conceptualization is the default mode network (DMN), which has also been associated with resting activity related to EEG alpha and theta (Kim et al., 2014; Pizzagalli, 2011; Qin et al., 2010). Despite these overlapping processes, it is unclear whether resting- and task-related EEG alpha provide comparable or complementary information. Moreover, since some measures are based solely on the eyes-closed EEG (e.g., Pizzagalli et al., 2001), it is not clear whether a condition-dependent blockade of resting alpha with eyes open (net alpha) provides an essential within-subject control (baseline comparison), rather just an unnecessary task demand. Inasmuch as individuals with a robust resting EEG alpha have a differential advantage following treatment with pharmacologic antidepressants (Bruder et al, 2008, 2013; Knott et al., 1996; Tenke et al, 2011; Ulrich et al., 1988), and may also show resilience following depression attributed to nonpharmacologic mechanisms (Tenke et al, 2013), individual differences in these measures have considerable importance for psychiatry.

The interpretability of measures of oscillatory activity can be profoundly affected by the choice of a recording reference (cf. Fig. 1 of Tenke and Kayser, 2005). Although the placement of a recording reference in proximity to known generators of alpha (e.g., parietal, occipital or occipitotemporal sites) would clearly introduce it into recordings

* Corresponding author at: New York State Psychiatric Institute, Division of Cognitive Neuroscience, Unit 50, 1051 Riverside Drive, New York, NY 10032, USA. Tel.: +1 646 774 5222.
E-mail address: cet2103@columbia.edu (C.E. Tenke).

http://dx.doi.org/10.1016/j.ijpsycho.2015.05.011
0167-8760/Published by Elsevier B.V.

from the entire montage, a common recording reference (AR) has long been acknowledged for its influence on synchrony measures (Fein et al., 1988; Guevara et al., 2005). Distortion in the amplitude topography of EEG alpha may also be expected using an average reference (AR; Tenke and Kayser, 2015). Even though Laplacian methods have been applied to EEG alpha (Nunez et al., 1997, 1999, 2001; Tenke et al., 2011), apprehensions about the attenuation or loss of global activity (Andrew and Pfurtscheller, 1997; Nunez et al., 2001; Nunez and Srinivasan, 2006) have had the unfortunate effect of dissuading researchers from its greater use, except as a supplement to reference-dependent measures. The result for the field has been the continued reliance on reference strategies that frequently differ across labs. It would therefore be of importance to conclusively determine whether concerns about the loss or distortion of resting- or task-related alpha amplitude measures are justified when using a surface Laplacian (current source density; CSD) based on a comparison with commonly used reference strategies.

In a simulation paper (Tenke and Kayser, 2015), we noted that a spherical spline Laplacian computed with rigid splines ($m \geq 5$) preserves activity from a broadly distributed posterior generator. Given that flexible splines ($m \leq 3$) approximate an analytical Laplacian, it is of critical importance that we also substantiated the loss of such distributed activity when flexible splines are used. However, the same simulations identified clear errors for AR at quiescent regions near the frontal pole. Unfortunately, the presence or absence of errors or distortions in a simulation may not be a convincing model for the widely-distributed empirical data produced by physiological alpha activity.

The primary goal of this report was to compare resting and task-related EEG alpha measures produced by a spherical spline Laplacian with intermediate flexibility ($m = 4$) with nose-referenced (NR) and AR transformations. To equally identify and document local and global properties, it was essential to compare complete topographies, for which we employed topographic randomization tests.

The secondary goal was to determine whether resting EEG alpha and task-related alpha measures obtained during a novelty oddball task are linked in a way that is consistent with a common mechanism underlying all rhythmic alpha activity. The demands of this task are not particularly great, and some individuals show considerable EEG alpha during it, suggesting that those who have the greatest resting condition-dependent alpha might also show the greatest condition-dependent alpha during task performance (i.e., task baseline vs alpha ERD). Since CSD can unambiguously distinguish posterior alpha measures of enduring significance (i.e., prediction of a patient's response to subsequent pharmacologic treatment for depression; Tenke et al., 2011), it was hypothesized that individual differences in resting alpha (i.e., topography, scatter and correlation) would closely correspond to those of task-related alpha. To this end, we also examined scatterplots and correlations of posterior resting alpha, task baseline alpha, and task alpha ERD.

2. Methods

2.1. Participants

Healthy participants[1] ($n = 49$; 23 male participants; mean age = 31 ± 10.6 years; mean education = 15.7 ± 2.6 years) with no history of psychopathology, current substance use disorders (including alcohol abuse), a history of head trauma, or other neurological disorders were recruited from the New York metropolitan area. Participants were screened using the Structured Clinical Interview for DSM-IV Axis I Disorders, Nonpatient Edition (First et al., 1996) to exclude those with current or past psychopathology. All participants were paid $15 per hour. The study was approved by the institutional review board, and all participants gave informed consent.

2.2. EEG tasks

2.2.1. Resting EEG task

Resting EEG was recorded while participants sat quietly in a sound attenuated booth. EEG was recorded during four 2-minute periods (eyes-closed [C] and eyes-open [O] counterbalanced across blocks: COOC or OCCO), with the condition order alternated across participants. Participants were instructed to remain still and to inhibit blinks or eye movements during each recording period. During the eyes-open condition, participants fixated on a central cross.

2.2.2. Novelty oddball task

An auditory novelty oddball task (Friedman et al., 1993; Tenke et al., 2010) consisted of eight 50-trial blocks of 300-ms tones (10 ms rise and fall time) and novel environmental sounds (100–400 ms duration) presented in pseudorandom order (1000 ms SOA). Unique novel sounds (e.g., animals, instruments; $p = .12$) were intermixed with frequent nontargets (350 Hz; $p = .76$) and infrequent targets (500 Hz; $p = .12$) presented binaurally at 85 dB SPL. Participants responded with a button press as quickly as possible when, and only when, they heard the infrequent target tone (response hand counterbalanced across blocks).

2.3. Electrophysiological procedures

2.3.1. EEG acquisition

The EEG was recorded using an electrode montage consisting of 67 expanded 10–20 system scalp channels (Pivik et al., 1993) on a Lycra stretch electrode cap (ActiveTwo EEG system; Biosemi Inc, 2001), including 10 midline sites and 28 homologous pairs over the left and right hemispheres, extending laterally to include the inferior temporal lobes (cf. Tenke et al., 2010). This recording system has an active recording reference composed of a common mode sense (at site PO1) and a driven right leg (at site PO2). Face electrodes were placed on the nosetip, which served as an online reference during acquisition, as well as at the external canthi and above and below the right eye. The electrode cap placement was optimized in all cases using direct measurements of electrode locations corresponding to landmarks of the 10–20 system (nasion, inion, auditory meatus, vertex). The scalp placements were prepared using a conventional water soluble electrolyte gel and the interface was verified by the acquisition software (ActiView; Biosemi Inc., 2001). Bipolar EOG recordings were computed and used to identify blinks and eye movements during visual inspection and validation of rejected artifacts.

Continuous EEG was acquired at 256 samples/s using the 24-bit Biosemi system and nose-referenced data were exported into 16-bit Neuroscan format using Polyrex (Kayser, 2003) to remove DC offsets, optimize data scaling, and rereference the EEG. Continuous EEG data were then blink corrected using a spatial, singular value decomposition (NeuroScan) and segmented into 2-s epochs every .5-s (75% overlap) for the resting EEG, or into stimulus-locked epochs (−200 to 1000 ms) for the novelty oddball task. Epoched data were then screened for electrolyte bridges (Alschuler et al., 2014; Tenke and Kayser, 2001). Channels containing artifacts or noise for any given trial were identified using a reference-free approach to identify isolated EEG channels containing amplifier drift, residual eye activity, muscle or movement-related artifacts for any given trial (Kayser and Tenke, 2006b), which were then replaced by spherical spline interpolations (Perrin et al., 1989) from artifact-free channels (i.e., if fewer than 25% of all channels contained artifact). Artifact detection and electrode interpolation was verified interactively. Performance for the Novelty task was 98.9 ± 1.8% correct, resulting in a total number of 224 ± 24 nontargets, 34 ±

[1] Grand mean ERP and CSD waveforms are shown for this sample and task in Tenke et al. (2010) and therefore reflect the quality of the data submitted to task-related alpha baseline and alpha ERD analyses in the present paper. The same sample also extensively overlapped (41 of 49 participants) the healthy controls in the resting EEG study of Tenke et al. (2011); (cf. supplementary Fig. S2 for grand mean amplitude spectra of CSD at midline and posterolateral sites).

5 targets and 31 ± 5 novels for each ERP average (minimum sweeps in any condition > 16). For the resting EEG, an additional automated step was included to reject any remaining epochs exceeding a ±100 μV threshold in any channel to conform to conventional methods. This resulted in a total of 320 ± 93 EEG epochs for eyes open and 253 ± 95 for eyes closed.

2.4. Resting EEG methods

Artifacted EEG epochs for each participant were rereferenced to nose (NR) or average (AR) reference. Likewise, reference-free current source density (CSD) epochs (μV/cm^2 units; 10 cm head radius) were computed using a spherical spline surface Laplacian (Perrin et al., 1989). The CSD transformation has been detailed elsewhere (Kayser and Tenke, 2006a, 2006b; available as Matlab-based CSD toolbox and tutorial; Kayser, 2009), and used the same parameters as in the original implementation (i.e., 50 iterations; $m = 4$; $\lambda = 10^{-5}$; Kayser and Tenke, 2006a, 2006b). Corresponding epochs (2 s; 75% overlap) of all three data transformations were tapered using a 50% Hanning window and padded with zeros (1 s at each end), submitted to FFT, and transformed to yield power spectra with a resolution of .25 Hz (Neuroscan software). The final spectral resolution was consistent with Tenke et al. (2011); (1 s epochs padded to 4 s; 1024 points/epoch), but with less spectral interpolation.

Power spectra were transformed (square root) to yield amplitude spectra (Tenke and Kayser, 2005) and the standard deviations of NR and AR were each scaled to match that of the CSD for overall alpha (8–12 Hz; both conditions) at 17 posterior sites where alpha is maximal (P7/8, P5/6, P3/4, P1/2, Pz, PO7/8, PO3/4, POz, O1/2, Oz). As illustrated in Fig. 1A (bottom spectra), this correction yields dimensionless amplitude spectra that adjust for the different scales of the three transformations measures for each waveform (66 electrodes × 2 conditions × 49 participant; nose channel removed). EEG alpha was quantified at each electrode site for net (eyes-closed minus eyes-open) and overall (eyes-closed plus eyes-open) alpha using the conventional 8–12 Hz alpha band.[2]

2.5. Novelty oddball task methods

ERSPs and corresponding baseline spectra were obtained for each data transformation (CSD, NR, AR) from stimulus-locked epochs (−200 to 1000 ms) for each electrode, condition (target, nontarget, novel) and participant using EEGlab (Delorme and Makeig, 2004). After zero-padding (4×), the baseline and ERSP matrices consisted of power spectra with 1 Hz resolution.

2.5.1. Task alpha measure

Baseline power spectra were converted to amplitude spectra for comparability with the resting spectra. After scaling the data from all three transformations to a common scale based on posterior alpha (Fig. 1A, top spectra), task alpha was quantified as the mean amplitude across the alpha band (8–12 Hz) for each transformation for all cases (66 electrodes × 3 conditions × 49 participants).

2.5.2. Alpha ERD measure

ERSP matrices were computed from FFT-based power spectra with 1 Hz resolution at −76.9 to 876.1 ms (EEGLAB; Delorme and Makeig, 2004), and expressed as log power changes from the task prestimulus baseline. The 29,106 ERSP surfaces resulting from the transformations (3), conditions (3), electrodes (66) and participants (49) were interpolated to 10 ms resolution (−70 to 800 ms; 1 to 50 Hz). The resulting ERSP surfaces for the three transformations were scaled as described above for the resting and task baseline measures. Alpha ERD was then computed as the mean across the 8–12 Hz band and across characteristic latencies (350 to 650 ms) for target-related ERD (rectangle in Fig. 1B; cf. Kayser et al., 2014) for correctly detected targets (i.e., the condition where it was maximal; Kayser et al., 2014).

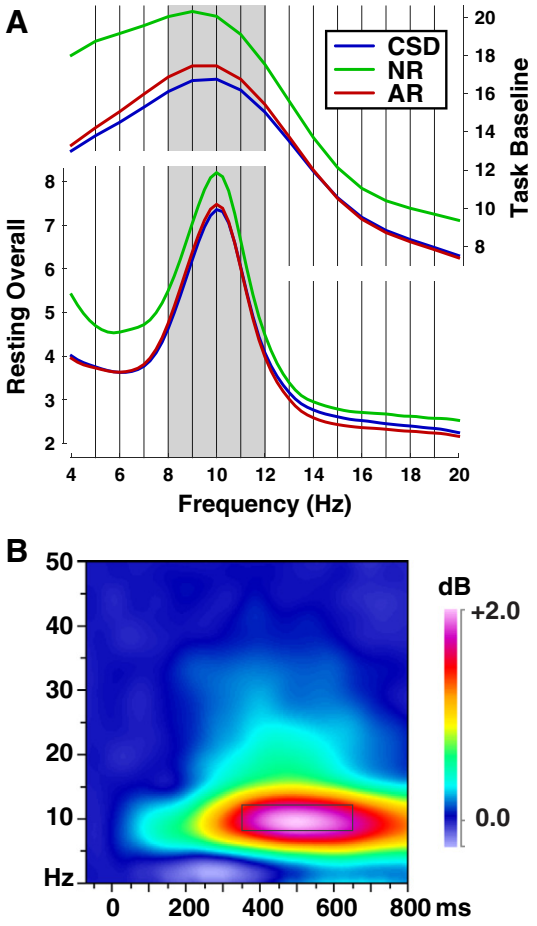

Fig. 1. EEG alpha at rest and during task performance for three data transformations: current source density (CSD), nose reference (NR), average reference (AR). Shown are means pooled across 17 posterior sites where alpha is maximal (P7/8, P5/6, P3/4, P1/2, Pz, PO7/8, PO3/4, POz, O1/2, Oz). Spectra from all transformations were scaled to equate their standard deviations across the 8–12 Hz alpha band with CSD. A. Mean amplitude spectra between 4 and 20 Hz at rest (overall represents sum of eyes open and closed) and during task baseline. The gray interval represents the 8–12 Hz alpha band used for all amplitude measures. B. Factor loadings surface of the highest variance time–frequency PCA factor (17.2%) jointly extracted from the post-stimulus CSD, NR and AR time–frequency plots in the novelty oddball task (for PCA methods, see Kayser and Tenke, 2015a, 2015b; Kayser et al., 2014). This surface efficiently represents alpha event-related spectral perturbations, being sharply confined to alpha, with a single 10 Hz peak at 500 ms post-stimulus (cf. Supplementary Fig. S1 to compare with mean time–frequency plot). The rectangle indicates the time–frequency window (350–650 ms, 8–12 Hz) used to measure alpha event-related desynchronization (ERD).

2.6. Statistical methods

2.6.1. Overview

The primary goal was to compare resting- and task-related EEG measures produced by CSD, NR and AR transformations, with particular attention to possible topographic distortions that might be caused by

[2] We report results using intuitive, band-based alpha measures that are widely-used in the field. Although static, pre-determined frequency bands are not as effective as frequency PCA at disentangling activity that spans across bands (Kayser and Tenke, 2003; Tenke and Kayser, 2005; Tenke et al., 2011), for the present purpose, the use of PCA-based methods is not necessary. In fact, the less-complex window-based measures allow a better focus on the cross-measure comparisons. Main findings were comparable for both methods.

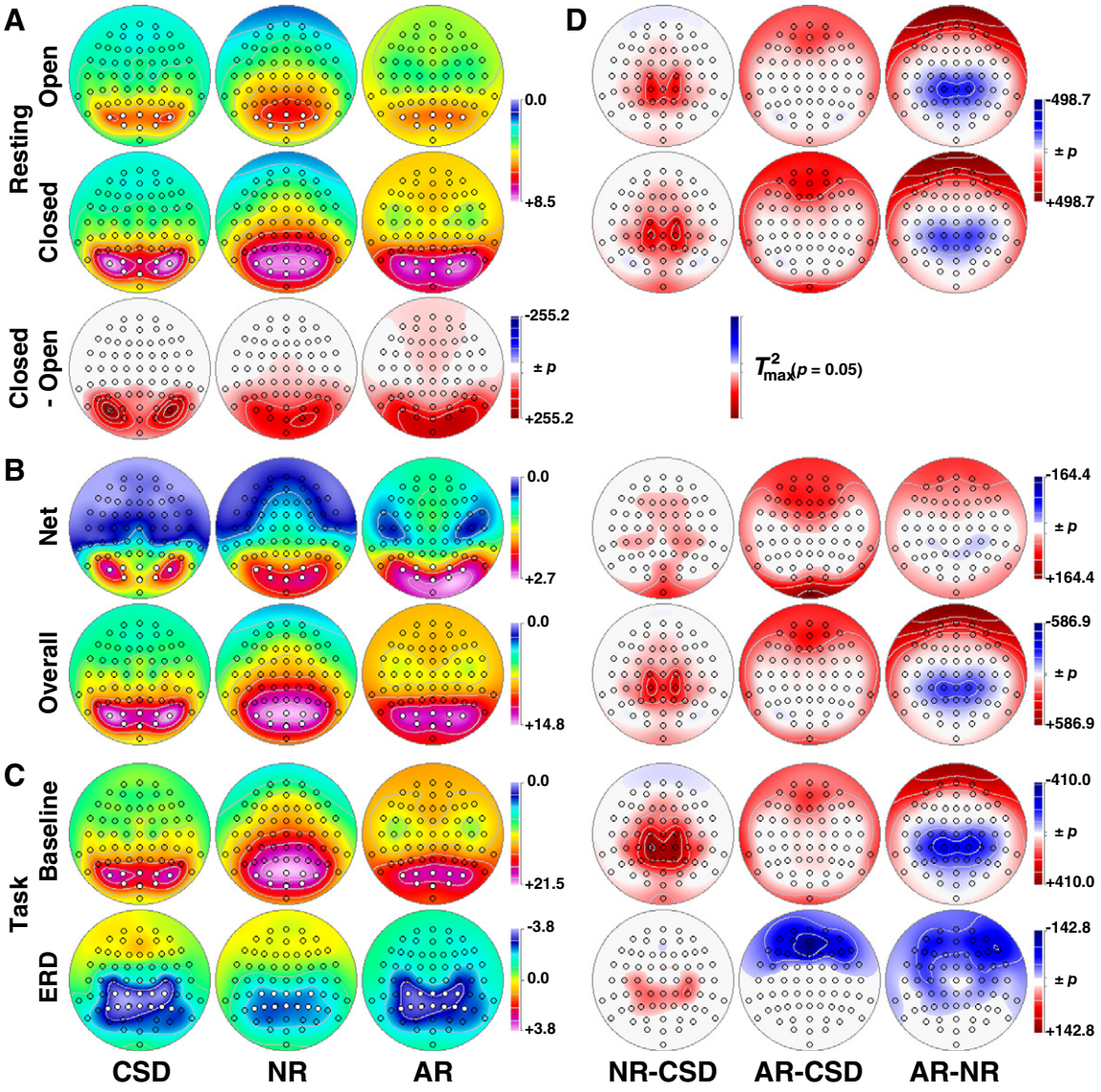

Fig. 2. Grand mean alpha (8–12 Hz) amplitude topographies for CSD, NR, and AR (cf. Fig. 1A). (A) Eyes-open and eyes-closed condition during rest. Sites used for posterior alpha analyses (occipitoparietal ROI) are marked. The bottom row (red–white–blue scale) maps the corresponding squared univariate (channel-specific) paired samples *T* statistics thresholded at the 95th quantile ($p \leq .05$ for red or blue regions) of the corresponding randomization distribution (maximum of all 66-channel squared univariate paired samples *T* statistics). To facilitate comparisons of the max (T^2) topographies with the underlying difference topographies, the sign of the difference at each site was applied to the respective T^2 value, which is otherwise always positive. (B) Overall and net alpha derived from eyes open and closed. (C) Prestimulus task baseline and target alpha ERD. (D). Pairwise significant tests of differences between transformations for each row of panels A–C. All transformations showed characteristic posterior topographies for overall and task alpha, with topographies for CSD being sharpest and NR most distributed. AR showed an intermediate distribution with a shallower falloff (less dark blue in panels A–C). All topographies in this report are two-dimensional representations of spherical spline interpolations ($m = 2$; $\lambda = 0$) derived from the values (i.e., amplitude, spectra, T^2 statistics) available for each recording site, at which quantified data are precisely represented.

the putative spatial selectivity of CSD for local over global activity. To accomplish this, grand mean topographies were computed and compared across transformations using unbiased randomization tests of differences at all electrode sites.

The secondary goal was to determine whether resting and task measures were linked in a way that is consistent with a common mechanism underlying all rhythmic alpha activity. This was also accomplished by comparing grand mean topographies of the alpha measures. Finally, posterior region-of-interest (ROI) estimates were used to evaluate the association between the resting and task alpha measures in individuals, and to evaluate the possibility of a mutual association that could enhance the empirical value of posterior alpha (e.g., as a predictor of antidepressant treatment response; Tenke et al., 2011).

2.6.2. Comparison of alpha topographies

Grand mean topographies were computed for each alpha measure (resting net and overall alpha, task baseline alpha and alpha ERD) and transformation (CSD, NR, AR). Net alpha was defined as the difference between eyes-closed and eyes-open resting conditions, and overall alpha as their sum, which is statistically equivalent to a transformation × condition interaction and a transformation main effect when employing a two within-subject factors repeated measures ANOVA design. The differential distribution of alpha was evaluated for pairwise differences using randomization distributions estimated from the observed data (Huo et al., 2013; Maris, 2004; Kayser et al., 2007). For each topographic comparison (i.e., between eyes open and closed conditions and between data transformations), the maximum

Table 1
Grand means (±*SD*) of posterior alpha (8–12 Hz) measures for each transformation and ANOVA *F* ratios.

		Occipitoparietal (8 sites)						Centroparietal (12 sites)	
Alpha measure[a]		Net		Overall		Task baseline		ERD	
CSD		1.79	±1.70	13.23	±5.69	17.66	±8.08	−3.36	±2.56
NR		2.04	±2.09	13.94	±5.47	19.92	±8.24	−2.34	±2.68
AR		2.16	±2.02	13.17	±5.78	18.10	±8.43	−3.12	±2.38
Effect[b]		F	*p*	F	*p*	F	*p*	F	*p*
Transformation[c]		6.46	.009	10.6	.0005	37.0	<.0001	39.4	<.0001
Contrasts	NR-CSD	3.83	.056	9.07	.004	38.2	<.0001	43.8	<.0001
	AR-CSD	9.64	.003			4.05	.05	9.51	.003
	AR-NR	5.44	.024	34.5	<.0001	63.3	<.0001	45.9	<.0001

[a] CSD: current source density; NR: nose reference; AR: average reference.
[b] For all effects, $df = 1, 48$. Only *F* ratios with $p < .10$ are reported.
[c] Greenhouse–Geisser adjusted *df*, $0.65758 \le \varepsilon \le 0.69677$.

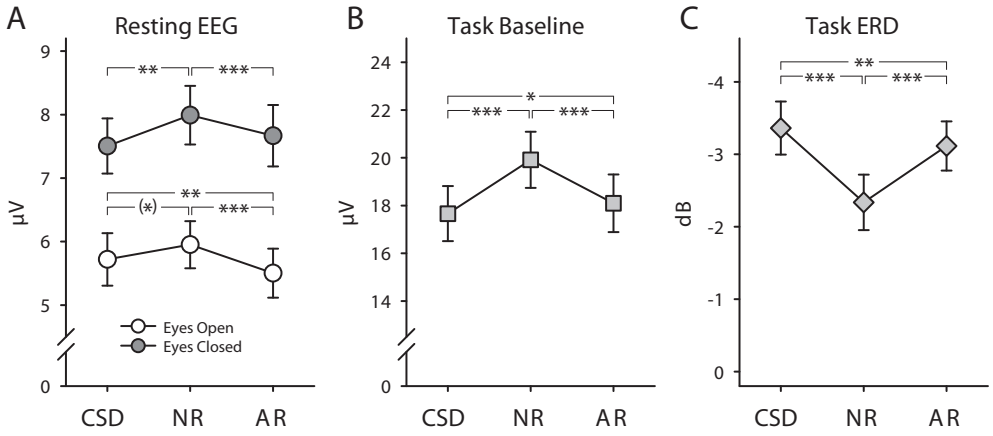

Fig. 3. Posterior 8–12 Hz alpha means (±SEM; $N = 49$) of three data transformations (CSD: current source density; NR: nose reference; AR: average reference) for (A) eyes open/closed during rest, (B) task baseline and (C) task event-related desynchronization (ERD). Means were pooled across 8 parietal–occipital sites (A, B) or 12 centroparietal sites (C; cf. sites marked in Fig. 2). Significant pairwise contrasts between transformations are marked with brackets (*** $p < 0.001$; ** $p < 0.01$; * $p < 0.05$; [*] $p < 0.10$).

randomization distribution (10,000 repetitions) of the univariate (channel-specific) T^2 statistic for paired samples (cf. Eq. 2 in Kayser et al., 2007) was computed after randomly multiplying the observed differences for each participant by +1 or −1 (Maris, 2004). Being an exploratory analysis, no control for family-wise error for the entire topography was needed.[3]

2.6.3. Posterior alpha measures

Occipitoparietal alpha amplitude measures were computed for resting and task baseline alpha as means across 8 occipitoparietal sites where alpha was maximal for all transformations (ROI: PO7/8, PO3/4, POz, O1/2, Oz). The ROI for the alpha ERD reflected a more anterior topography including 12 centroparietal sites (ROI: CP3/4, CP1/2, CPz, P5/6, P3/4, P1/2, Pz). The adequacy of ROIs for each transformation was evaluated based on the corresponding grand mean topographies, as well as their underlying variance distribution (using PCA factor score topographies).

Because these posterior alpha measures differed in their underlying data distribution, their units and the ROIs across which they were pooled, separate repeated measures ANOVAs were performed for: 1) net resting alpha, 2) overall resting alpha, 3) task baseline alpha, and 4) alpha ERD, using transformation (CSD, NR, AR) as a within-subject design factor in order to evaluate whether alpha amplitude estimates differ between transformations. An additional analysis was performed for resting alpha, using condition (eyes open/closed) and transformation (CSD, NR, AR) as within-subject design factors, which allowed the evaluation of the condition × transformation interaction. Simple effects and pairwise contrasts (BMDP-4V; Dixon, 1992) were used to examine sources of interactions. When appropriate, Greenhouse–Geisser epsilon (ε) correction was used to compensate for violations of sphericity (e.g., Keselman, 1998). A conventional significance level ($p < .05$) was applied for all effects.

Posterior alpha measures were also compared across subjects using pairwise scatterplots, and the direction and strength of their associations quantified by product–moment correlations. Three-way scatterplots were also created for net, overall and task alpha, but are described only for CSD, owing to the similarity across transformations. As an additional descriptive aid for visualizing the impact of these associations on complete topographies, maps were also computed for subgroups based on their respective medians, and the corresponding contingency tables computed.

3. Results

3.1. Grand mean topographies and statistical differences

Fig. 2A shows grand mean alpha topographies for eyes-open and eyes-closed conditions for each transformation, as well as the randomization tests of their differences in the sample of participants

[3] It must be noted that the corresponding multivariate test statistics for the complete 66-channel topography would require a minimum of 68 participants (i.e., number of EEG montage channels + 2; Maris, 2004). Although restricting the analyses to those identified with the ROIs for alpha leads to robust closed-minus-open differences (net for each transformation, $T^2 \ge 8.26$, $p < .0001$), these multivariate T^2 statistics do not provide meaningful information above the reported pattern of univariate max(T^2) statistics resulting for the randomization of complete topographies (see Kayser et al., 2007).

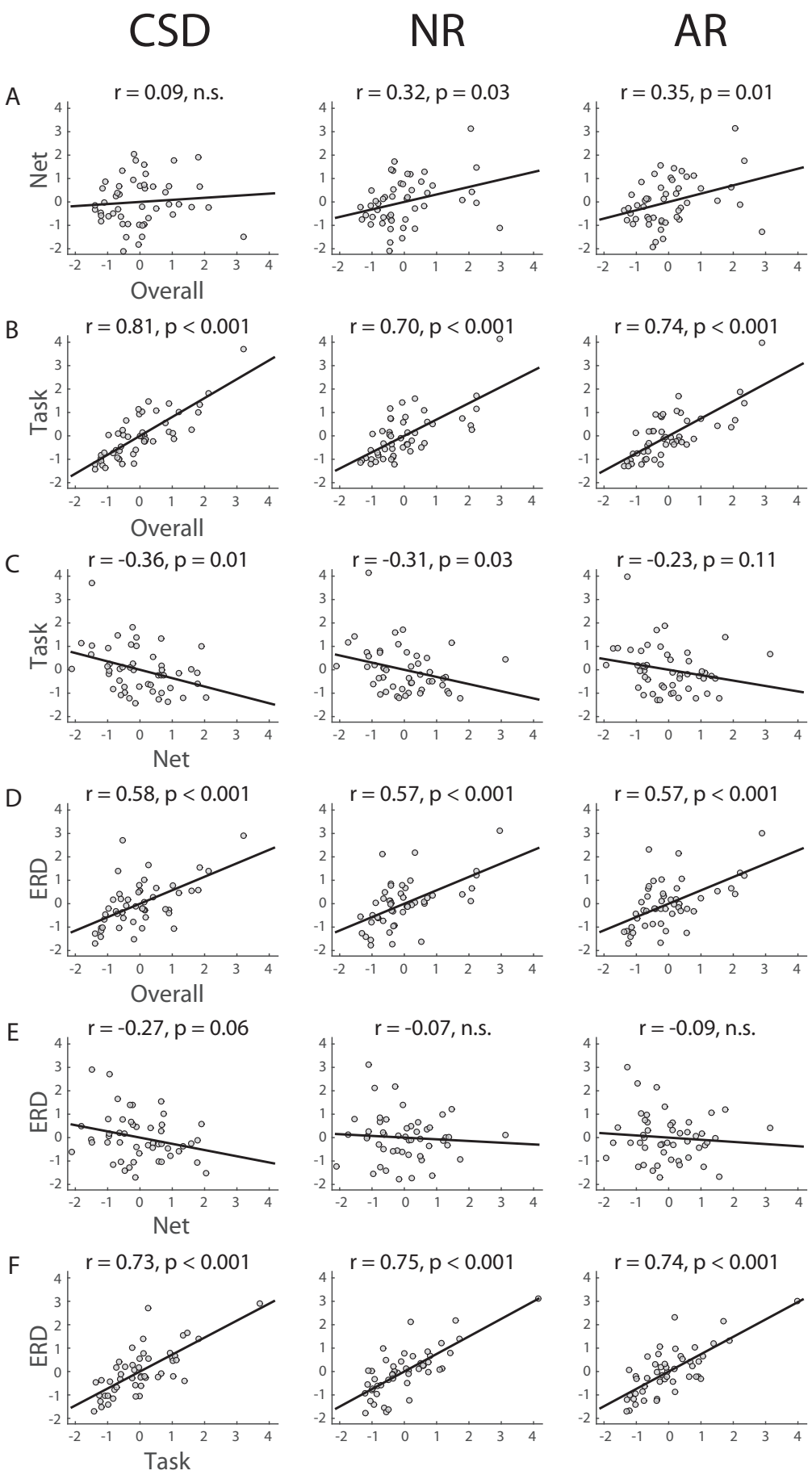
CSD
NR
AR
A
r = 0.09, n.s.
r = 0.32, p = 0.03
r = 0.35, p = 0.01
Net
Overall
B
r = 0.81, p < 0.001
r = 0.70, p < 0.001
r = 0.74, p < 0.001
Task
Overall
C
r = -0.36, p = 0.01
r = -0.31, p = 0.03
r = -0.23, p = 0.11
Task
Net
D
r = 0.58, p < 0.001
r = 0.57, p < 0.001
r = 0.57, p < 0.001
ERD
Overall
E
r = -0.27, p = 0.06
r = -0.07, n.s.
r = -0.09, n.s.
ERD
Net
F
r = 0.73, p < 0.001
r = 0.75, p < 0.001
r = 0.74, p < 0.001
ERD
Task

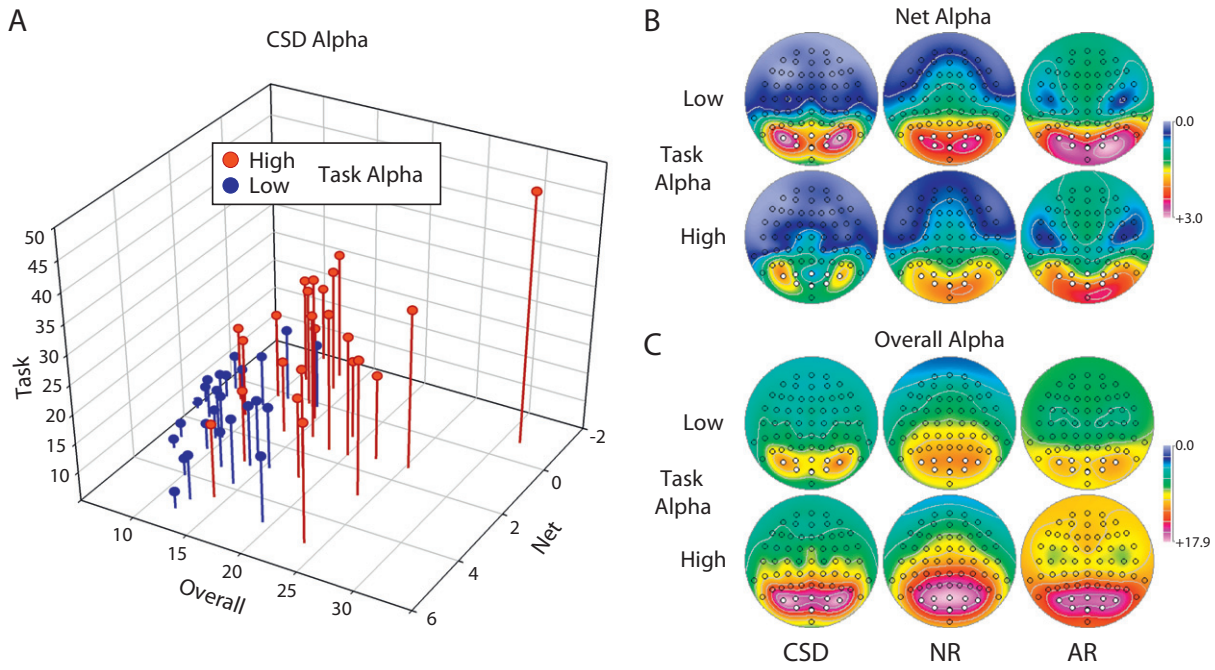

Fig. 5. Association between overall, net and task alpha amplitude across participants. A. Scatterplot of posterior CSD measures of overall, task and net alpha for all participants. Participants with greater task alpha than the median are indicated in red to facilitate visualization of the association between measures. The net axis is reversed for clarity, due to the prevalence of high task alpha among participants with low net alpha. The positive correlation between overall and net alpha in the remaining participants (blue) is also apparent. B. Using the task groupings shown in A, it is evident that only participants with low task alpha show the expected posterior topography of net alpha. C. In contrast, the same task groupings show that participants with high task alpha also have prominent overall posterior alpha.

(i.e., net alpha; bottom row, red–white maps). The randomization maps were thresholded at $p = .05$, so that all visible colors represent greater than threshold (i.e., significant) differences, with deeper colors indicating the most robust differences. For all three transformations, net alpha showed a robust posterior topography, with the topographies of CSD being sharpest and of NR being the most diffuse.

In contrast to CSD and NR, AR showed frontal net alpha. Fig. 2D shows the randomization tests of pairwise differences between transformations (red–white–blue maps in the three rightmost columns). The clearest property of all of these probability maps is that the significant differences between transformations are notably not in areas where alpha is prominent (i.e., the posterior region identified by the closed-minus-open comparisons), but rather in adjacent anterior areas (red areas in NR-minus-CSD; blue areas in AR-minus-NR) where alpha would be expected to volume conduct. Again, AR was unique in identifying frontal alpha (red areas in AR-minus-CSD and AR-minus-NR). Despite these robust differences between transformations, it is also clear that each of the pairwise differences between transformations was essentially identical for eyes closed and eyes open.

These data are expressed as overall and net (condition-dependent) grand mean topographies in Fig. 2B (left three columns), showing the marked differences between them. For both CSD and NR transformations, anterior alpha is eliminated. For AR, net alpha is only nulled at lateral sites, with a substantial frontal contribution remaining. The posterior net alpha maximum for NR is slightly posterior to that for overall and task alpha, and even more so for the AR. In marked contrast, the corresponding posterior maximum for the CSD transformation is identical to that observed for overall and task alpha.

The similarity of the net grand mean topographies (Fig. 2B, top row) and the corresponding randomization tests (row directly above Fig. 2B) is evident, as is the similarity between the overall grand mean (Fig. 2B, bottom row) and eyes closed maps (Fig. 2A, row 2). Moreover, for overall alpha the pairwise randomization tests between transformations (Fig. 2D, same row) are indistinguishable from those for eyes-open or -closed alone (Fig. 2D, rows 1 and 2). Only net alpha differs, because of a notable reduction of anterior spread for NR (less red for NR-minus-CSD; less blue for AR-minus-NR). For AR, the frontal area extends further posterior to frontocentral sites (red in AR-minus-CSD and AR-minus-NR).

Fig. 2C shows the grand mean topographies of the task baseline alpha and the alpha ERD to target stimuli. The similarity overall resting and task baseline alpha is striking, with NR showing a midline maximum, CSD an off-midline maximum, and AR an intermediate posterior topography. Although no transformation precluded a minor representation at frontocentral sites, only the AR suggested that the frontal contribution was large (i.e., >50% maximum over an extended region). The corresponding three pairwise randomization topographies (Fig. 2D, second from bottom row) were also similar to overall alpha, but different from net alpha.

As previously reported (Kayser et al., 2014), alpha ERD is predominantly anterior to posterior alpha, being most pronounced at centroparietal sites (blue areas in Fig. 2C, bottom row). In contrast to the greater diffusion of task baseline alpha for NR compared with CSD, there was less alpha ERD for NR than for CSD (i.e., NR-minus-CSD marked red and AR-minus-ERD marked blue over centroparietal sites in Fig. 2D, bottom row). However, an apparent frontal contribution to alpha ERD

Fig. 4. Pairwise scatterplots of net and overall resting alpha, task baseline and task ERD (sign inverted to aid comparison across alpha measures) are shown for each of the three transformations (CSD, NR, AR). All measures were standardized (z-scores) to account for their different scales. Product–moment correlations were similar across transformations, being positive and significantly different from zero for all correlations except for those involving net alpha.

was again evident only for AR (anterior blue regions in AR-minus-CSD and AR-minus-NR in Fig. 2D, bottom row).

3.2. ANOVA statistics of posterior differences

Although the randomization tests provide an effective and powerful nonparametric method to evaluate topographic differences, the repeated measures ANOVA results for the posterior alpha measures (Table 1) may be used to directly evaluate the differences between the transformations across their associated ROIs (cf. Fig. 2B and C). These F-tests identified robust transformation effects for all measures. In contrast to this inclusive difference pattern, AR and CSD did not differ significantly for overall posterior alpha, and were only marginally different for task baseline posterior alpha (see contrasts in Table 1). For net posterior alpha, the difference between AR and CSD was the most robust.

Fig. 3 shows the difference between transformations for the raw (i.e., uncombined) resting EEG and task alpha. For resting alpha, a condition main effect, $F[1,48] = 54.4$, $p < .0001$, confirmed the greater alpha for eyes closed than open (i.e., net alpha), and a transformation main effect, $F[2,96] = 10.6$, $p < .001$, $\varepsilon = 0.6968$, as well as transformation × condition interaction, $F[2,96] = 6.46$, $p < .01$, $\varepsilon = 0.6339$, indicated that both overall alpha amplitude and strength of net alpha varied with transformation (note that two-way interaction and the transformation main effect are equal to the transformation effects for net and overall alpha already reported in Table 1). While the simple condition effects were highly significant for each transformation (all $F[1,48] \geq 46.8$, all $p < .0001$), the pairwise contrasts between transformations for each condition did not show a significant difference between CSD and AR for eyes closed, and only a marginal difference between CSD and NR for eyes open (Fig. 3A), which together accounted for the primary source of this two-way interaction. For overall alpha, NR showed the largest posterior resting alpha amplitude (contrasts: NR vs. CSD, $F[1,48] = 9.07$, $p = .004$; NR vs. AR, $F[1,48] = 34.5$, $p < .0001$), while CSD and AR did not differ ($F[1,48] < 1.0$, *n.s.*).

Almost the same difference between transformation was observed for task baseline alpha ($F[2,96] = 37.0$, $p < .0001$, $\varepsilon = 0.6576$). While NR also had greatest posterior alpha amplitude (contrasts: NR vs. CSD, $F[1,48] = 38.2$, $p < .0001$; NR vs. AR, $F[1,48] = 63.3$, $p < .0001$), the greater alpha amplitude of AR compared to CSD was less robust ($F[1,48] = 4.05$, $p < .05$; Fig. 3B).

In contrast, alpha ERD was greatest for CSD, followed by AR, which was greater than NR (Fig. 3C; transformation main effect, $F[2,96] = 39.4$, $p < .0001$, $\varepsilon = 0.6679$; contrasts: CSD vs. NR, $F[1,48] = 43.8$, $p < .0001$; CSD vs. AR, $F[1,48] = 9.51$, $p = .003$; NR vs. AR, $F[1,48] = 63.3$, $p < .0001$).

3.3. Association between alpha measures at occipitoparietal sites

Fig. 4A–C shows pairwise scatterplots combining the three occipitoparietal alpha measures for each transformation. Although overall and task alpha show a robust correlation for all transformations, correlations involving net alpha are poor (net × overall) or negative (task × net). This relationship is also evident in the joint scatterplot of Fig. 5 (net, overall and task; to avoid redundancy, only CSD data are shown). As a descriptive tool for visualizing these differences, individuals are coded as high or low task alpha, based on median task alpha as a classifier. It is apparent that participants with high task alpha (red; largest stems on plot) are distinct from those with low task alpha, accounting for all of the participants with a net alpha of zero or less (i.e., individuals for which the usual closed-minus-open condition effect is missing or inverted). Using the same descriptive approach, Table 2 shows the same data arranged as contingency tables based on the joint medians of each grouping, stratified by net alpha.[4] Although all of these tables indicate significant associations between overall and task alpha, the association was most robust for individuals with prominent net alpha (i.e., >median).

Fig. 5B and C show mean topographies for net and overall alpha based on these ad hoc subgroups, showing that only participants with low task alpha showed the expected net resting alpha topographies (i.e., greater alpha with eyes closed than with eyes open). In sharp contrast, overall resting alpha was most prominent for participants with high task alpha. A related observation is that the exclusion of participants with high task alpha in Fig. 5A leads to a substantial increase in the correlation between the two resting measures (net, overall) for the remaining participants (low task alpha: $r = .51$, $p < .02$; high task alpha: $r = .29$, $p > .1$).

3.4. Relationship between ERD and resting or task baseline alpha

Fig. 4D–F shows the pairwise scatterplots of the occipitoparietal alpha measures with the centroparietal alpha ERD for each transformation. All correlations were again robust and positive with the exception of those involving net, which (nonsignificantly) trended negative. Fig. 6 illustrates the three-way association between posterior measures of task and overall resting alpha amplitude and the alpha ERD, again using task median alpha as a descriptive tool for visualizing these differences (only CSD shown as an example). Fig. 7 illustrates these corresponding maps as a descriptive tool to visualize these complete topographies that correspond to these differences. Again, task alpha amplitude and ERD were greater for participants with high overall alpha and low net alpha.

4. Discussion

4.1. Impact of data transformation on the topography of alpha

The present study indicates that empirical, reference-dependent EEG recordings may be simply and directly compared with their corresponding reference-independent CSD. In all cases, the differences between these transformations were directly comparable, and consistent with predictions from simulations of distributed subdural generators (Tenke and Kayser, 2015). CSD topographies were more sharply-defined, while maxima for NR were more broadly distributed. The AR topography was intermediate, showing regional differentiation consistent with that shown by the CSD. However, the AR topography also had a flattened amplitude range, a long-recognized computational consequence of the AR that leads to an erroneous secondary maximum at midfrontal regions (compare Fig. 2 with Figs. 4 and 7 of Tenke and Kayser, 2015). This finding indicates that the use of CSD computed with moderate spline flexibility is comparable to AR for alpha amplitude estimates (Fig. 3), but is superior to AR in its representation of the complete alpha topography. Although overall and net resting alpha and task prestimulus alpha amplitudes all had consistent topographies across the sample, task and overall alpha were the most stable and most similar, with NR estimates being more robust than the other transformations.

Although we have reported that the volume conduction weakens the representation of neuronal generator patterns evidenced by scalp potentials when compared to CSD topographies (e.g., Kayser and Tenke, 2015a; Tenke and Kayser, 2015), we must consider the possibility that the redundancy introduced by volume conduction into field potentials may inflate the signal in regions that would otherwise be dominated by background noise. However, only NR means for occipitoparietal alpha consistently exceeded those for CSD, indicating that the difference was not due to the preservation of low spatial frequencies by field potential transformations per se. A relevant distinction between NR and AR is that only NR computationally defines activity at or near the nose to zero, making it noise-free and 'correct' for a topography dominated by distributed posterior generators (Tenke and Kayser, 2015). The apparent superiority of NR therefore cannot be generalized

[4] Rearrangement of Table 2 to stratify by task alpha showed no association between the resting measures (low task alpha: $p = .6$; high task alpha: $p = .06$; total: $p = .77$).

Table 2
Contingency tables for net, overall and task alpha (median splits).

		Task		
Net	Overall	<Median	>Median	Total
<Median	<Median	7	6	13
($p = .033$)[a]	>Median	1	10	11
	Total	8	16	24
	Overall	<Median	>Median	Total
>Median	<Median	12	0	12
($p = .002$)[a]	>Median	5	8	13
	Total	17	8	25
	Overall	<Median	>Median	Total
Total	<Median	19	6	25
($p = .001$)[a]	>Median	6	18	24
	Total	25	24	49

[a] 2-Tail Fisher's exact test.

to phenomena with substantially different neuronal generator patterns (e.g., ERP components).

4.2. How many posterior alphas are there?

Apart from the comparison of the three transformations, the present findings provide insight into the significance of common measures of alpha in the resting EEG, as well as their relationship to task-related alpha. Resting- and task-related EEG alpha amplitudes are sufficiently correlated and comparable in topography to suggest a common origin. In contrast, the task-related alpha ERD topographies are more anterior, with a bilateral extension into centroparietal sites that is not present for the other measures, suggesting a separate contribution from the central mu rhythm. Although task prestimulus alpha amplitude and the subsequent ERD might be expected to be correlated with each other, the association with overall resting alpha is by no means self-evident, indicating a persistent (trait-like) individual difference that spans the two recording periods. However, we also observed marked differences between net and overall resting alpha in relation to task-related alpha: overall resting alpha paralleled task-related measures, but net (i.e., condition-dependent) resting alpha tended to oppose them. A plausible interpretation of this difference emphasizes the difference between the modest attentional requirements of a resting EEG as compared to the effortful nature of task performance. For resting EEG, alpha is *blocked* when visual attention (to the fixation mark) is imposed, but neither condition requires the engagement of the individual. In contrast, task-related prestimulus alpha occurs within an effortful task that requires engagement and attention. The findings of Fig. 5 may be accounted for by supposing that participants with high amplitude alpha during the novelty task were not sufficiently engaged to show an alpha blockade (i.e., net alpha) during the resting "task." This distinction also challenges the supposition that *condition-dependent* posterior resting alpha (i.e., net alpha) provides a better estimate by virtue of the within-subject "baseline" provided by eyes-open alpha. This supposition is clearly violated by participants who show EEG alpha at rest with no blockade, suggesting that condition *independent* posterior resting alpha (i.e., overall alpha) may be of greater importance to behavior.

These findings also have direct implications for activity in the default mode network, which was originally posited in the context of imaging studies as the base activity on which task-related effects are overlaid (e.g., Gusnard and Raichle, 2001; Raichle et al., 2001). The same conceptualization has been applied to the resting EEG, particularly in the context of psychopathology (Kim et al., 2014; Pizzagalli, 2011). It should be recognized that the distinction between net and overall alpha cannot be made in EEG studies in which only eyes-closed resting alpha is recorded. Although we previously reported on the value of net resting alpha as a predictor of antidepressant treatment response (Tenke et al., 2011), in a longitudinal study of participants at high or low risk for depression, overall posterior resting alpha distinguished between individuals classified according to personal spirituality, and thereby with resilience

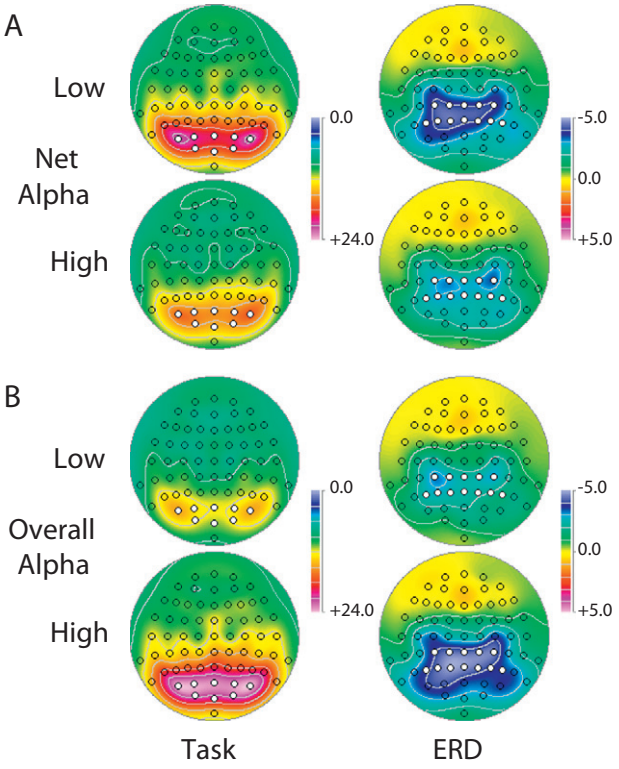

Fig. 7. CSD topographies of prestimulus (task) and poststimulus (ERD) alpha for median-split groupings based on overall and net alpha amplitude. A. By virtue of the association demonstrated in Fig. 4, participants with high overall alpha also show a prominent task alpha and equally prominent poststimulus alpha ERD. B. Due to the overrepresentation of high task alpha among individuals with low net alpha (Fig. 3A), prominent task alpha amplitude and the subsequent alpha ERD are only observed for participants with low net alpha. Note that the sites used for the statistical analysis of alpha ERD were more anterior than those used for alpha amplitudes (as indicated).

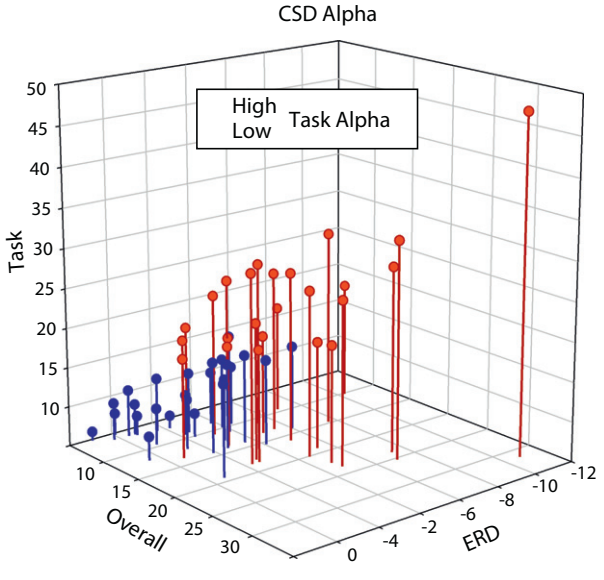

Fig. 6. Scatterplot of regional CSD measures of task and overall alpha amplitude and alpha ERD for all participants. Participants with greater task alpha than the median are indicated in red to facilitate visualization of the association between measures. The ERD axis is reversed for clarity, owing to the correspondence between high prestimulus (task) alpha task and the subsequent ERD (desynchronization is negative). In contrast to Fig. 3A, all three measures are correlated (i.e., the classification threshold is arbitrary).

following depression (Tenke et al., 2013). The distinction between overall and net alpha clearly requires additional study, and might have implications for nonpharmacologic interventions which have the capacity to alter EEG alpha at rest and during cognitive or affective tasks. Just as task alpha indexed the "decorrelation" of the two resting measures, so might alpha changes indicate a mechanism underlying resilience or affectivity that is amenable to behavioral therapies.

4.3. Conclusions and outlook

CSD provided more sharply defined, reference-free topographies that more closely represent the neuronal generator patterns from which they are derived than do NR or AR. Most importantly, CSD topographies and measures computed with our standard parameters (i.e., $m = 4$, $\lambda = 10^{-5}$) showed no evidence that they were "missing" information that was not merely volume-conducted. NR and CSD measures were entirely consistent, with AR showing intermediate regional localization, as well as discrepancies accountable for by computational misallocation (Tenke and Kayser, 2015). Although we are confident of the generalizability of these findings to other EEG phenomena, we acknowledge the possibility of topographic distortion when surface Laplacian estimates are computed using an overly flexible spline (e.g., $m = 2$; see Kayser and Tenke, 2015b; Tenke and Kayser, 2015). The present findings are promising, but they must be followed up with studies focusing on regional phase-locking, synchronization and coherence.

Supplementary data to this article can be found online at http://dx.doi.org/10.1016/j.ijpsycho.2015.05.011.

Acknowledgments

This research was supported in part by grants MH036295 and MH094356 from the National Institute of Mental Health (NIMH). We greatly appreciate helpful comments of Robert J. Barry and three anonymous reviewers.

References

Alschuler, D.M., Tenke, C.E., Bruder, G.E., Kayser, J., 2014. Identifying electrode bridging from electrical distance distributions: a survey of publicly-available EEG data using a new method. Clin. Neurophysiol. 125 (3), 484–490.
Andrew, C., Pfurtscheller, G., 1997. On the existence of different alpha band rhythms in the hand area of man. Neurosci. Lett. 222, 103–106.
Babiloni, C., Del Percio, C., Arendt Nielsen, L., Soricelli, A., Romani, G.L., Rossini, P.M., Capotosto, P., 2014. Cortical EEG alpha rhythms reflect task-specific somatosensory and motor interactions in humans. Clin. Neurophysiol. 125 (10), 1936–1945.
Barry, R.J., Kirkaikul, S., Hodder, D., 2000. EEG alpha activity and the ERP to target stimuli in an auditory oddball paradigm. Int. J. Psychophysiol. 39 (1), 39–50.
BioSemi, Inc., 2001. ActiveTwo — Multichannel, DC Amplifier, 24-bit Resolution, Biopotential Measurement System with Active Electrodes. Author, Amsterdam, NL (http://www.biosemi.com).
Bruder, G.E., Sedoruk, J.P., Stewart, J.W., McGrath, P.J., Quitkin, F.M., Tenke, C.E., 2008. Electroencephalographic alpha measures predict therapeutic response to a selective serotonin reuptake inhibitor antidepressant: pre- and post-treatment findings. Biol. Psychiatry 63 (12), 1171–1177.
Bruder, G.E., Tenke, C.E., Kayser, J., 2013. Electrophysiological predictors of clinical response to antidepressants. In: Mann, J.J., Roose, S.P., McGrath, P.J. (Eds.), The Clinical Handbook for the Management of Mood Disorders. Cambridge University Press, New York, pp. 380–393.
Delorme, A., Makeig, S., 2004. EEGLAB: an open source toolbox for analysis of single-trial EEG dynamics including independent component analysis. J. Neurosci. Methods 134 (1), 9–21.
Dixon, W.J. (Ed.), 1992. BMDP Statistical Software Manual: To Accompany the 7.0 Software Release. University of California Press, Berkeley, CA.
Fein, G., Raz, J., Brown, F.F., Merrin, E.L., 1988. Common reference coherence data are confounded by power and phase effects. Electroenceph. Electroencephalogr. Clin. Neurophysiol. 69 (6), 581–584.
First, M.B., Spitzer, R.L., Gibbon, M., Williams, J.B.W., 1996. Structured Clinical Interview for DSM-IV Axis-I Disorders — Non-patient Edition (SCID-NP). Biometrics Research Department, New York State Psychiatric Institute, New York, NY.
Friedman, D., Simpson, G., Hamberger, M., 1993. Age-related changes in scalp topography to novel and target stimuli. Psychophysiology 30 (4), 383–396.
Gloor, P., 1969. Hans Berger and the discovery of the electroencephalogram. Electroencephalogr. Clin. Neurophysiol. Suppl. 28, 1–36.
Guevara, R., Velazquez, J.L., Nenadovic, V., Wennberg, R., Senjanovic, G., Dominguez, L.G., 2005. Phase synchronization measurements using electroencephalographic recordings: what can we really say about neuronal synchrony? Neuroinformatics 3 (4), 301–314.
Gusnard, D.A., Raichle, M.E., 2001. Searching for a baseline: functional imaging and the resting human brain. Nat. Rev. Neurosci. 2 (10), 685–694.
Huo, M., Heyvaert, M., Van den Noortgate, W., Onghena, P., 2013. Permutation tests in the educational and behavioral sciences: a systematic review. Methodology 1–17 http://dx.doi.org/10.1027/1614-2241/a000067 (May 13. Online first publication).
Jasiukaitis, P., Hakerem, G., 1988. The effect of prestimulus alpha activity on P300. Psychophysiology 25 (2), 157–165.
Kayser, J., 2003. Polygraphic Recording Data Exchange — PolyRex. Department of Biopsychology, New York State Psychiatric Institute (http://psychophysiology.cpmc.columbia.edu/PolyRex.htm).
Kayser, J., 2009. Current source density (CSD) interpolation using spherical splines — CSD Toolbox (Version 1.1). Division of Cognitive Neuroscience, New York State Psychiatric Institute (http://psychophysiology.cpmc.columbia.edu/Software/CSDtoolbox).
Kayser, J., Tenke, C.E., 2003. Optimizing PCA methodology for ERP component identification and measurement: theoretical rationale and empirical evaluation. Clin. Neurophysiol. 114 (12), 2307–2325.
Kayser, J., Tenke, C.E., 2006a. Principal components analysis of Laplacian waveforms as a generic method for identifying ERP generator patterns: I. Evaluation with auditory oddball tasks. Clin. Neurophysiol. 117 (2), 348–368.
Kayser, J., Tenke, C.E., 2006b. Electrical distance as a reference-free measure for identifying artifacts in multichannel electroencephalogram (EEG) recordings. Psychophysiology 43, S51 (http://psychophysiology.cpmc.columbia.edu/mmedia/spr2006/ElecDistArti.pdf).
Kayser, J., Tenke, C.E., 2015a. Hemifield-dependent N1 and event-related theta/delta oscillations: an unbiased comparison of surface Laplacian and common EEG reference choices. Int. J. Psychophysiol. 97 (3), 258–270 (this issue).
Kayser, J., Tenke, C.E., 2015b. Issues and considerations for using the scalp surface Laplacian in EEG/ERP research: a tutorial review. Int. J. Psychophysiol. 97 (3), 189–209 (this issue).
Kayser, J., Tenke, C.E., Gates, N.A., Bruder, G.E., 2007. Reference-independent ERP old/new effects of auditory and visual word recognition memory: joint extraction of stimulus- and response-locked neuronal generator patterns. Psychophysiology 44 (6), 949–967.
Kayser, J., Tenke, C.E., Kroppmann, C.J., Alschuler, D.M., Fekri, S., Ben-David, S., Corcoran, C.M., Bruder, G.E., 2014. Auditory event-related potentials and alpha oscillations in the psychosis prodrome: neuronal generator patterns during a novelty oddball task. Int. J. Psychophysiol. 91 (2), 104–120.
Keselman, H.J., 1998. Testing treatment effects in repeated measures designs: an update for psychophysiological researchers. Psychophysiology 35 (4), 470–478.
Kim, J.S., Shin, K.S., Jung, W.H., Kim, S.N., Kwon, J.S., Chung, C.K., 2014. Power spectral aspects of the default mode network in schizophrenia: an MEG study. BMC Neurosci. 15, 104 (http://www.biomedcentral.com/1471-2202/15/104).
Klimesch, W., 2012. α-band oscillations, attention, and controlled access to stored information. Trends Cogn. Sci. 16 (12), 606–617.
Knott, V.J., Telner, J.I., Lapierre, Y.D., Browne, M., Horn, E.R., 1996. Quantitative EEG in the prediction of antidepressant response to imipramine. J. Affect. Disord. 39 (3), 175–184.
Maris, E., 2004. Randomization tests for ERP topographies and whole spatiotemporal data matrices. Psychophysiology 41 (1), 142–151.
Nunez, P.L., Srinivasan, R., 2006. Electric Fields of the Brain: The Neurophysics of EEG. Oxford University Press, New York.
Nunez, P.L., Srinivasan, R., Westdorp, A.F., Wijesinghe, R.S., Tucker, D.M., Silberstein, R.B., Cadusch, P.J., 1997. EEG coherency. I: Statistics, reference electrode, volume conduction, Laplacians, cortical imaging, and interpretation at multiple scales. Electroencephalogr. Clin. Neurophysiol. 103 (5), 499–515.
Nunez, P.L., Silberstein, R.B., Shi, Z., Carpenter, M.R., Srinivasan, R., Tucker, D.M., Doran, S.M., Cadusch, P.J., Wijesinghe, R.S., 1999. EEG coherency II: experimental comparisons of multiple measures. Clin. Neurophysiol. 110 (3), 469–486.
Nunez, P.L., Wingeier, B.M., Silberstein, R.B., 2001. Spatial–temporal structures of human alpha rhythms: theory, microcurrent sources, multiscale measurements, and global binding of local networks. Hum. Brain Mapp. 13 (3), 125–164.
Perrin, F., Pernier, J., Bertrand, O., Echallier, J.F., 1989. Spherical splines for scalp potential and current density mapping. Electroencephalogr. Clin. Neurophysiol. 72 (2), 184–187 (Corrigenda EEG 02274, EEG Clin. Neurophysiol., 1990, 76, 565).
Pivik, R.T., Broughton, R.J., Coppola, R., Davidson, R.J., Fox, N., Nuwer, M.R., 1993. Guidelines for the recording and quantitative analysis of electroencephalographic activity in research contexts. Psychophysiology 30 (6), 547–558.
Pizzagalli, D.A., 2011. Frontocingulate dysfunction in depression: toward biomarkers of treatment response. Neuropsychopharmacology 36 (1), 183–206.
Pizzagalli, D., Pascual-Marqui, R.D., Nitschke, J.B., Oakes, T.R., Larson, C.L., Abercrombie, H.C., Schaefer, S.M., Koger, J.V., Benca, R.M., Davidson, R.J., 2001. Anterior cingulate activity as a predictor of degree of treatment response in major depression: evidence from brain electrical tomography analysis. Am. J. Psychiatry 158, 405–415.
Qin, Y., Xu, P., Yao, D., 2010. A comparative study of different references for EEG default mode network: the use of the infinity reference. Clin. Neurophysiol. 121 (12), 1981–1991.
Raichle, M.E., MacLeod, A.M., Snyder, A.Z., Powers, W.J., Gusnard, D.A., Shulman, G.L., 2001. A default mode of brain function. Proc. Natl. Acad. Sci. U. S. A. 98 (2), 676–682.
Steriade, M., McCormick, D.A., Sejnowski, T.J., 1993. Thalamocortical oscillations in the sleeping and aroused brain. Science 262 (5134), 679–685.
Steriade, M., 2000. Corticothalamic resonance, states of vigilance and mentation. Neuroscience 101 (2), 243–276.

Tenke, C.E., Kayser, J., 2001. A convenient method for detecting electrolyte bridges in multichannel electroencephalogram and event-related potential recordings. Clin. Neurophysiol. 112 (3), 545–550.
Tenke, C.E., Kayser, J., 2005. Reference-free quantification of EEG spectra: combining current source density (CSD) and frequency principal components analysis (fPCA). Clin. Neurophysiol. 116 (12), 2826–2846.
Tenke, C.E., Kayser, J., 2015. Surface Laplacians and phase properties of EEG rhythms: simulated generators in a volume-conduction model. Int. J. Psychophysiol. 97 (3), 285–298 (this issue).
Tenke, C.E., Kayser, J., Stewart, J.W., Bruder, G.E., 2010. Novelty P3 reductions in depression: characterization using principal components analysis (PCA) of current source density (CSD) waveforms. Psychophysiology 47 (1), 133–146.
Tenke, C.E., Kayser, J., Manna, C.G., Fekri, S., Kroppmann, C.J., Schaller, J.D., Alschuler, D.M., Stewart, J.W., McGrath, P.J., Bruder, G.E., 2011. Current source density measures of electroencephalographic alpha predict antidepressant treatment response. Biol. Psychiatry 70 (4), 388–394.
Tenke, C.E., Kayser, J., Miller, L., Warner, V., Wickramaratne, P., Weissman, M.M., Bruder, G.E., 2013. Neuronal generators of posterior EEG alpha reflect individual differences in prioritizing personal spirituality. Biol. Psychol. 94 (2), 426–432.
Ulrich, G., Haug, H.J., Stieglitz, R.D., Fähndrich, E., 1988. EEG characteristics of clinically defined on-drug-responders and non-responders—a comparison clomipramine vs. maprotiline. Pharmacopsychiatry 21 (6), 367–368.
von Stein, A., Chiang, C., König, P., 2000. Top-down processing mediated by interareal synchronization. Proc. Natl. Acad. Sci. U. S. A. 97 (26), 14748–14753.